ACS Energy LETTERS

Cite This: ACS Energy Lett. 2018, 3, 2669−2670

http://pubs.acs.org/journal/aelccp

ENERGY EXPRESS

Subgrain Special Boundaries in Halide Perovskite Thin Films Restrict Carrier Diffusion

Wenhao Li,[†,‡] Srinivas K. Yadavalli,[†] David Lizarazo-Ferro,[†,‡] Min Chen,[†] Yuanyuan Zhou,[†] Nitin P. Padture,[†] and Rashid Zia*[,†,‡]

[†]School of Engineering, [‡]Department of Physics, Brown University, 184 Hope Street, Providence, Rhode Island 02912, United States

Supporting Information

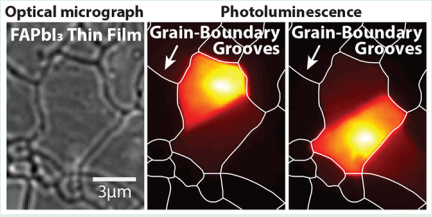

ABSTRACT: Photoluminescence microscopy reveals subgrain special boundaries in $FAPbI_3$ perosvkite thin films that restrict carrier diffusion and serve as nonradiative recombination sites. These subgrain boundaries, which cannot be observed by conventional AFM or SEM measurements of grain-boundary grooves, may explain why the performance of perovskite solar cells has not scaled with apparent grain size.

Perovskite solar cells (PSCs) based on organic−inorganic halide perovskite (OIHP) materials have attracted considerable attention in recent years because of their rapidly increasing power-conversion efficiency (PCE) that currently exceeds 23%.[1] Given that most high-efficiency PSCs are made of polycrystalline films, grain size is an important microstructural feature to characterize,[2] because grain boundaries can reduce PCE by limiting carrier diffusion and introducing nonradiative recombination sites. Since grain-boundary grooves form naturally during OIHP film growth,[2] many techniques for identifying grain boundaries rely on surface morphology characterization, for example, using atomic force microscopy (AFM) or scanning electron microscopy (SEM).[3] However, not all boundaries exhibit clear surface features. Here, we demonstrate the existence of special subgrain boundaries in formamidinium lead iodide ($HC(NH_2)_2PbI_3$ or $FAPbI_3$) perovskite thin films that cannot be observed by either AFM or SEM but which present significant barriers for carrier transport.

Panels a−c of Figure 1 show representative optical, SEM, and AFM images of a large-grained $FAPbI_3$ pervoskite thin film produced by low-temperature solvent-vapor annealing.[4] On the basis of the visible grain-boundary grooves, one might assume that the central ("penguin"-shaped) feature is a single grain. To study this feature, we examine the spatially resolved photoluminescence (PL) intensity distribution for focused laser excitation at 532 nm. Superimposed onto the SEM image, panels d and e of Figure 1 show the resulting PL images for excitation by a near-diffraction-limited ∼250 nm spot located in the top and bottom regions, respectively. Note that the luminescent areas are much larger than the excitation spot, because carriers can diffuse prior to recombination. Both PL images show a sharp straight discontinuity that bisects the feature and clearly prevents carrier diffusion, consistent with prior work showing

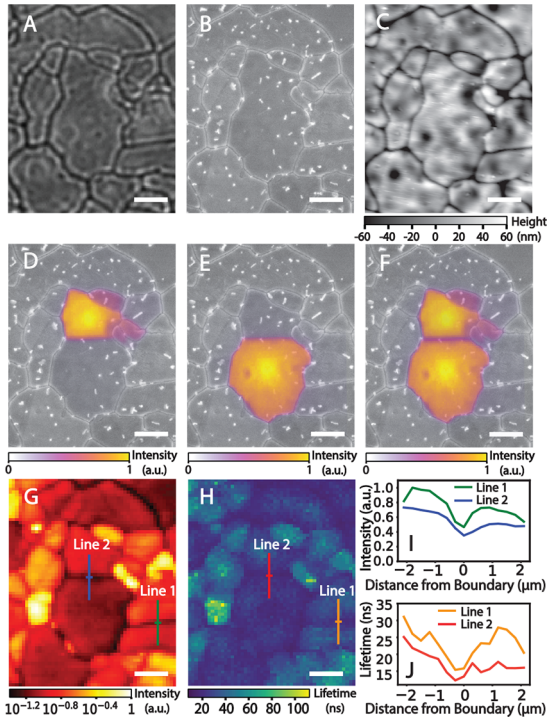

Figure 1. Top-surface images of $FAPbI_3$ perovskite thin film obtained by (a) optical microscopy, (b) SEM, and (c) AFM measurements. (d−f) Focused excitation PL intensity distributions superimposed onto the SEM image. Scanning confocal (g) PL intensity and (h) PL lifetime maps. All scale bars are 3 μm. (i and j) Averaged PL intensity and lifetime comparison between boundaries with (line 1) and without (line 2) visible grooves.

Received: September 10, 2018
Accepted: October 4, 2018
Published: October 4, 2018

DOI: 10.1021/acsenergylett.8b01704
ACS Energy Lett. 2018, 3, 2669−2670

reduced carrier transport across visible grain-boundary grooves.[5,6] However, in this case, there is no visible surface feature at this sharp discontinuity. Using the relative PL intensity drop as a qualitative indicator for carrier diffusion and connectivity,[5] it is also interesting to note that carriers in Figure 1d appear to diffuse more readily across the visible grain-boundary grooves on the right-hand side than they do across the invisible subgrain discontinuity.

Superimposing the PL images for excitation in the top and bottom regions, as shown in Figure 1f, we observe that this straight line is associated with reduced PL intensity across the entire apparent grain. To study carrier recombination, we use scanning confocal microscopy to record time-resolved PL emission as a function of excitation position across the sample. Figure 1g,h demonstrates that this line is associated with a reduced PL intensity and shortened carrier lifetime, comparable to that observed at nearby grain-boundary grooves (see Figure 1i,j). These results show that this carrier transport boundary, which is invisible to AFM or SEM characterization, is associated with significant nonradiative recombination.

We readily observed similar carrier transport boundaries in all large-grained $FAPbI_3$ perovskite thin film samples that we measured. Figure 2 shows several more examples. While these

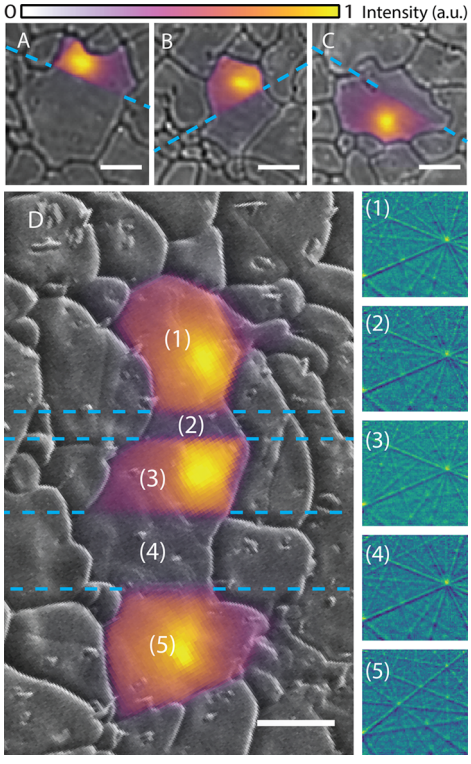

Figure 2. PL intensity distribution images for four different apparent grains superimposed onto optical microscopy images (a−c) and SEM image (d). Dashed blue lines highlight the special boundaries, and all scale bars are 3 μm. Right-hand images in panel d show EBSD Kikuchi patterns from regions labeled 1−5.

boundaries often bisect the grain into two regions, Figure 2d highlights an example where an apparent grain is segmented into five regions by four such boundaries (plain SEM image is available in the Supporting Information). In contrast to normal grain boundaries, these boundaries are straight, parallel, and groove-less. Their parallel nature suggests that these sharp discontinuities are special boundaries, reminiscent of twin boundaries found in other perovskite materials.[7] To study the relative crystal orientations of the subgrain regions, we acquired spatially resolved electron backscatter diffraction (EBSD) Kikuchi patterns across the sample and then averaged these patterns for each of the five labeled regions. While the average EBSD pattern for region 5 is unique, regions 1−4 exhibit identical Kikuchi patterns. This suggests that their crystallographic orientation is closely related (either identical or rotated by a symmetry angle). While further characterization will be necessary to determine their precise crystallographic nature, it is clear from the EBSD and PL data that these special boundaries are coherent, akin to twin boundaries.

As evidenced by the PL data, the significant impact of these special boundaries on carrier transport may help explain why PSC device performance has not scaled with apparent grain size.[8,9] While further investigation is required to quantify the prevalence and impact of special boundaries for other OIHP materials, the results presented here show that PL microscopy can provide a powerful (rapid and nondestructive) means of revealing these otherwise invisible boundaries and characterizing their effects on carrier transport for large-grained OIHP films.

■ ASSOCIATED CONTENT

Supporting Information

The Supporting Information is available free of charge on the ACS Publications website at DOI: 10.1021/acsenergylett.8b01704.

Experimental procedures and additional data (PDF)

■ AUTHOR INFORMATION

Corresponding Author

*E-mail: Rashid_Zia@brown.edu.

ORCID

Min Chen: 0000-0002-8655-5642

Nitin P. Padture: 0000-0001-6622-8559

Rashid Zia: 0000-0002-2742-5186

Notes

The authors declare no competing financial interest.

■ ACKNOWLEDGMENTS

The authors thank Dr. H. Sternlicht and Dr. A. Chatterjee for useful discussions and Dr. W. Moberlychan at Oxford Instruments for help acquiring the EBSD data. Funding was provided by the National Science Foundation (OIA-1538893) and the Office of Naval Research (N00014-17-1-2232).

■ REFERENCES

(1) National Renewable Energy Laboratory (NREL). Best Research-Cells Efficiencies Chart. 2018; https://www.nrel.gov/pv/assets/pdfs/pv-efficiencies-07-17-2018.pdf (accessed Sept 2018).
(2) Zhou, Y.; et al. *J. Phys. Chem. Lett.* **2015**, *6*, 4827−4839.
(3) Thompson, C. V. *Annu. Rev. Mater. Sci.* **2000**, *30*, 159−190.
(4) Yadavalli, S. K.; et al. *ACS Energy Lett.* **2018**, *3*, 63−64.
(5) deQuilettes, D. W.; et al. *ACS Nano* **2017**, *11*, 11488−11496.
(6) Snaider, M. J.; et al. *ACS Energy Lett.* **2018**, *3*, 1402−1408.
(7) Rothmann, M. U.; et al. *Nat. Commun.* **2017**, *8*, 14547.
(8) Saliba, M.; et al. *Angew. Chem., Int. Ed.* **2018**, *57*, 2554−2569.
(9) Huang, J.; et al. *J. Phys. Chem. Lett.* **2015**, *6*, 3218−3227.

DOI: 10.1021/acsenergylett.8b01704
ACS Energy Lett. 2018, 3, 2669−2670